Dalton Transactions

Cite this: *Dalton Trans.*, 2011, **40**, 9512

www.rsc.org/dalton

PAPER

Synthesis of a chloro protected iridium nitrido complex†

Daniel Sieh, Julia Schöffel and Peter Burger*

Received 10th May 2011, Accepted 15th July 2011
DOI: 10.1039/c1dt10886g

Intramolecular activation processes of vulnerable ligand C–H bonds frequently limit the thermal stability and accessibility of late transition metal complexes with terminal metal nitrido units. In this study chloro substitution of the 2,6-ketimine N-aryl substituents (2,6-$C_6H_3R_2$, R = Cl) of the pyridine, diimine ligand is probed to increase the stability of square-planar iridium nitrido compounds. The thermal stability of iridium azido precursor and nitrido compounds was studied by a combination of thermoanalytical methods (DTG/MS and DSC) and were compared to the results for the related complexes with 2,6-dialkyl substituted N-aryl groups (R = Me, iPr). The investigations were complemented by DFT calculations, which allowed us to unravel details of the thermal decomposition pathways and provided mechanistic insights of further conversion steps and fluctional processes. The DTG/MS and DSC measurements revealed two different types of thermolysis pathways for the azido compounds. For the complexes with R = Cl and iPr substituents, two well-separated exothermic processes were observed. The first moderately exothermic loss of N_2 is followed by a second, strongly exothermic transformation. This contrasts the experimental results for the compound with 2,6-dimethyl substituents (R = Me), where both steps proceed concurrently in the same temperature range. The separation of the two thermal steps in the 2,6-dichloro substituted derivative allowed us to develop a protocol for the isolation of the highly insoluble nitrido complex, which was characterized by UV/vis, IR-spectroscopy and elemental analysis. Its constitution was further confirmed by reaction with silanes, which gave the corresponding silyl amido complexes.

Introduction

In low valent late transition metal complexes with a terminal nitrido unit, $L_nM{\equiv}N$, 4 electron two orbital destabilizing interactions between the strong π-donor nitrido ligand and occupied metal orbitals are anticipated to lead to highly reactive intermediates.[1] Caulton *et al.* reported the structural characterization of a d^4-configured Ru nitrido complex in 2005,[2] which was succeeded by the isolation of iron complexes with the same electron configuration.[3] We have recently published the synthesis, X-ray crystallographic characterization and reactivity of a square-planar pyridine, diimine iridium nitrido complex. Based on experimental XAS and XPS measurements and detailed theoretical investigations including multi-reference calculations we rationalized a d^6-electron configuration for this compound with a terminal nitrido unit.[4]

Complexes of this type show interesting reactivity patterns that were explored only in the last few years. The dimerization to bridged dinitrogen complexes according to 2 $L_nM{\equiv}N \rightarrow L_nM{-}N_2{-}ML_n$ is a well-established reaction pathway,[5] which can be prevented[6] by the use of sterically demanding ligands shielding the terminal metal nitrido unit. Further prominent examples include the intermolecular formation of ammonia by H atom abstraction,[7] the activation of main group hydrides[8] and molecular hydrogen.[4] Frequently, intramolecular deactivation steps of highly reactive putative or isolated metal imido[9] and nitrido[10] units by insertion into benzylic and arylic C–H bonds is observed. For the aforementioned isolated iridium nitrido complex, we recently reported the thermal intramolecular activation of a benzylic C–H bond leading to the corresponding "tuck-in" amido complex.[11] Warren *et al.* showed that these undesirable intramolecular steps can be prevented by chloro substitution of the *vulnerable* C–H bonds.[9] Taking up this concept, we herein report the synthesis and thermolysis of the 2,6-chloro aryl protected pyridine, diimine iridium azido complex **4-Cl**. Its thermal stability will be compared to the 2,6-methyl substituted analogue **4-Me**, which has a similar sterical demand of the ligand.

Results and discussion

Syntheses

The synthesis of the chloro substituted ligand **1** was initially attempted by a previously reported route of Qian *et al.*[12] Following

Institut für Anorganische und Angewandte Chemie Universität Hamburg, Martin-Luther-King-Platz 6, 20146 Hamburg, Germany. E-mail: burger@chemie.uni-hamburg.de; Fax: (+49) 40 42838 6097; Tel: (+49) 40 42838 3662

† Electronic supplementary information (ESI) available: Further details of the thermoanalytical experiments, selected UV/vis, IR and NMR spectra of isolated and indistinct complexes and the DFT optimized geometries including total energies. CCDC reference numbers 825841–825845. For ESI and crystallographic data in CIF or other electronic format see DOI: 10.1039/c1dt10886g

their procedure, however, we had significant problems to isolate the product from the resulting brown oil. Applying a small modification, *i.e.* using benzene instead of toluene as solvent, allowed us to isolate ligand **1** in 29% yield after crystallization from acetone. This also provided single crystals suitable for X-ray crystallography, which was performed to analyze changes within the ligand upon coordination. The molecular structure of ligand **1** is shown in Fig. 1, selected bond lengths are given in the figure caption. Further details of the crystal data and structure refinement for compound **1** and the other crystal structures presented in this work are summarized in Table 4 and in the X-ray crystallography section. The solid state structure of ligand **1** shows *E*-configurations for both imine double bonds with regard to the aryl and pyridine groups. This is in agreement with previous findings for pyridine, diimine ligands.[12,13] The pyridine, diimine N-donors belong to the well-established class of non-innocent ligands. They undergo significant changes of the bond distances of the exocyclic pyridine C–C and imine C–N double bonds in their transition from the innocent to non-innocent state. The averaged bond lengths of 1.28 Å for the C–N double bonds of the imine units (N1–C2, N3–C8) and the averaged bond distances of 1.50 Å for the exocyclic C–C bonds of the pyridine ring are therefore relevant benchmarks for the innocent behaviour of this ligand (*cf.* below).

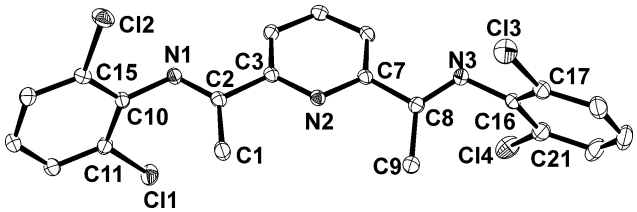

Fig. 1 Ortep representation of ligand **1** with anisotropic displacement parameters shown at 50% probability level. Hydrogen atoms are omitted for clarity. Selected bond lengths [Å] with esd's in parentheses: N1–C2 1.281(2), N1–C10 1.415(2), N3–C8 1.277(2), N3–C16 1.413(2), N2–C3 1.342(2), N2–C7 1.348(2), Cl1–C11 1.739(1), Cl2–C15 1.742(1), Cl3–C17 1.742(2), Cl4–C21 1.743(2), C1–C2 1.505(2), C2–C3 1.500(2), C3–C4 1.396(2), C4–C5 1.389(2), C5–C6 1.388(2), C6–C7 1.394(2), C7–C8 1.497(2), C8–C9 1.500(2), C10–C11 1.404(2), C10–C15 1.395(2), C16–C17 1.400(2), C16–C21 1.395(2).

Using a standard protocol,[14–16] the rhodium and iridium chlorido compounds **2-Rh** and **2-Ir** were obtained in analytically pure form and in moderate to good yields (Scheme 1). The ^{1}H and ^{13}C NMR data of the chlorido compounds **2-Rh,Ir** were consistent with the anticipated pseudo square-planar C_{2v}-symmetrical geometries for d^{8}-systems, which was unambiguously confirmed by the sum of angles of the Rh center of 359.99° observed in the X-ray crystal structure of complex **2-Rh**. The molecular structure of **2-Rh** is displayed in Fig. 2, details of the data collection and structural solution are summarized in Table 4, selected geometrical parameters in Table 1. The effects of the oxidation state of the metal center and the donor properties of the additional ligands on the geometrical parameters of the pyridine, diimine donor in **2-Rh** will be discussed below in context with the molecular structures obtained in this study.

It should be noted that compared to analogous complexes with 2,6-dialkyl substituents, the dichloro derivatives **2–5** show a substantially lower solubility in organic solvents, *e.g.* toluene, Et_2O or THF. The chlorido complexes **2-Rh,Ir**, for example, are

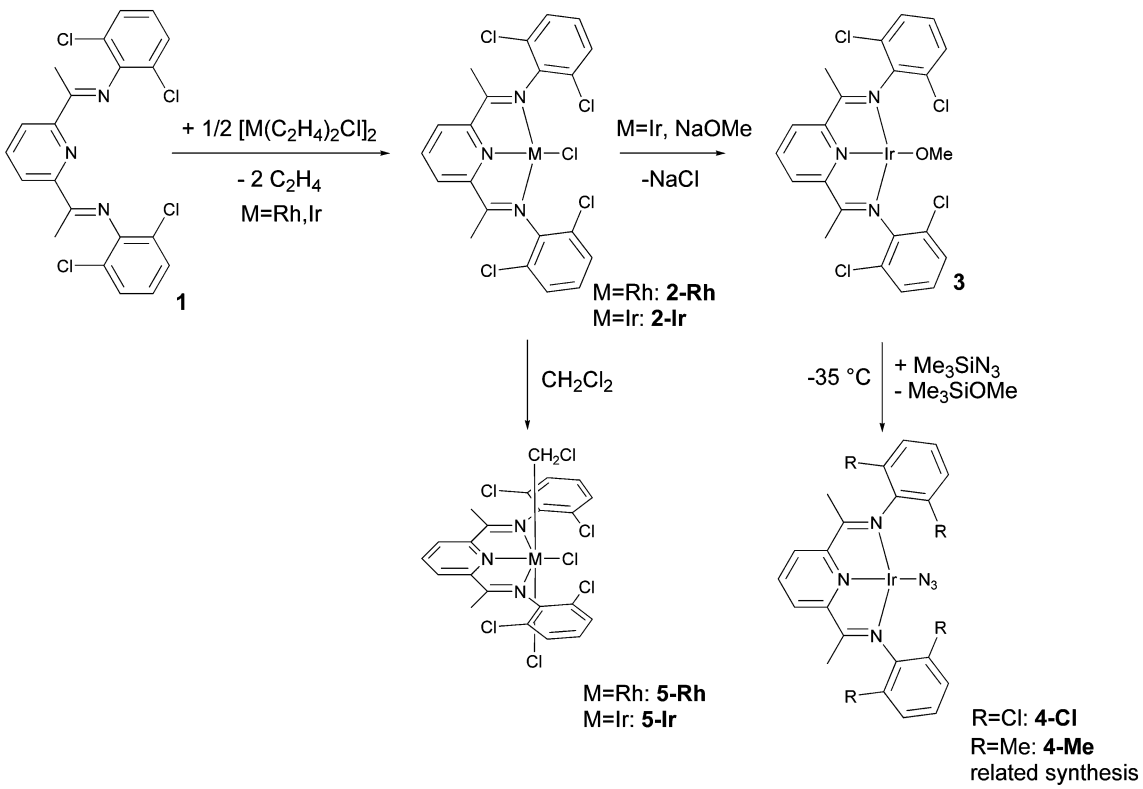

Scheme 1 Synthesis and reactivity of the rhodium and iridium complexes **2–5**.

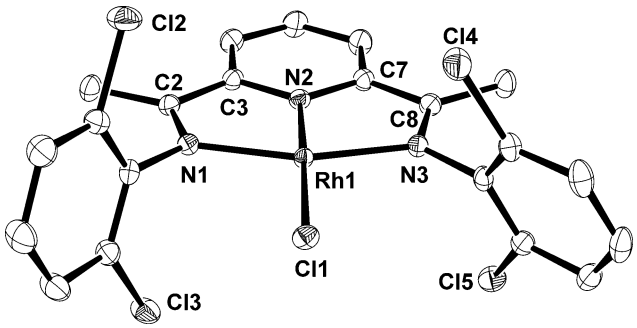

Fig. 2 Ortep plot (50% probability level) for the molecular structure of **2-Rh**. Hydrogen atoms and the co-crystallized THF molecule are omitted for clarity.

Table 1 Selected bond lengths (Å) and angles (°) of **2-Rh**[a]

Rh1–N1	2.0168(14)	Rh1–N2	1.8915(14)
Rh1–N3	2.0323(14)	Rh1–Cl1	2.3211(4)
N1–C2	1.315(2)	N3–C8	1.316(2)
C2–C3	1.457(2)	C7–C8	1.457(2)
N1–Rh1–N3	158.34(6)	N2–Rh1–Cl1	178.77(5)
N1–Rh1–N2	79.03(6)	N1–Rh1–Cl1	99.74(4)
N2–Rh1–N3	79.32(6)	N3–Rh1–Cl1	101.90(4)

[a] Esd's in parentheses.

only slightly soluble in THF and display reasonable solubility only in dichloromethane.

In the course of the NMR spectroscopic characterization we noted that the rhodium and iridium chlorido compounds **2-Rh,Ir** react at room temperature within several hours with the dichloromethane solvent to give the corresponding octahedral complex **5-Rh,Ir** under oxidative addition. This type of reaction was previously also observed for pyridine, diimine Rh(I) complexes.[14] Upon warming the solution to 55 °C the reaction goes to completion to give **5-Rh** and **5-Ir** in 88% and 95% isolated yields. In the aromatic range of the ^{1}H NMR spectrum of **5-Rh** and **5-Ir**, two well separated regions for the pyridine and phenyl rings centered at *ca.* 8 ppm and 7.4 were detected. For the three protons of the 2,6-dichloro phenyl groups three sets of signals in a 1 : 1 : 1 integration ratio were observed. This suggested a diastereotopic situation for the protons in the 3 and 5 positions, which is caused by the absence of a mirror plane or C_2-axis located within the framework of the pyridine, diimine N-donors and the iridium center. On the other hand, the observation of a singlet for the (enantiotopic) ketimine methyl resonances implied a mirror plane perpendicular to the ligand framework. Based on these results C_s-symmetry was anticipated for **5-Rh** and **5-Ir**, which required placement of the chloromethyl group (CH_2Cl) in the apical position of the octahedron with a cis-configuration of the remaining two chlorido ligands. This assignment was unambiguously confirmed by the results of the X-ray crystal structure analyses of complexes **5-Rh** and **5-Ir**, which evidenced a distorted octahedral coordination around the rhodium and iridium metal centers. The isostructural molecular structures of the complexes **5-Rh** and **5-Ir** are presented in Fig. 3, details of the data collection, structure solution and refinement are tabulated in Table 4, selected geometrical parameters in Table 2. The bonding parameters are essentially identical for both the iridium and the rhodium system. Since the quality of the crystal structure **5-Rh** is significantly higher, the data will be discussed only for the latter. By comparison with the bonding parameters in the free ligand **1**, only negligible differences of the C–N and C–C distances of the diimine group and the exocyclic C–C bond of the pyridine group clearly speak in favour of an innocent pyridine, diimine ligand

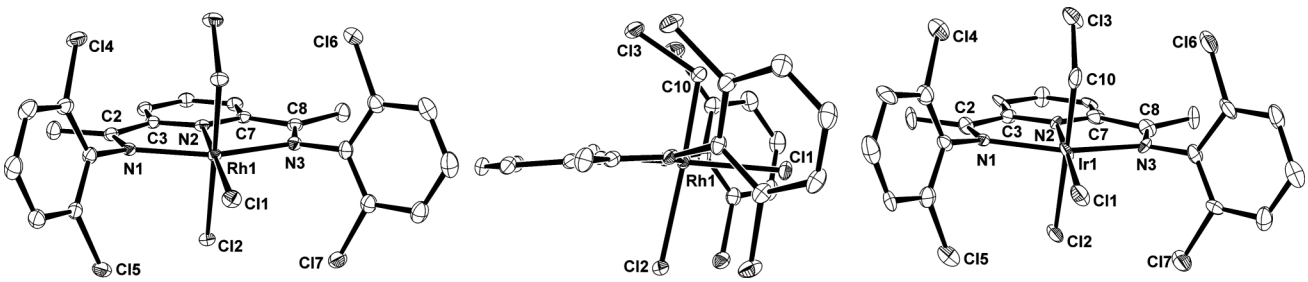

Fig. 3 Front and side view of the Ortep representation of the octahedral complexes **5-Rh** and **5-Ir** with anisotropic displacement parameters shown at 50% probability level. The hydrogen atoms and a co-crystallized CH_2Cl_2 molecule are omitted for clarity.

Table 2 Selected bond lengths (Å) and angles (°) of **5-Rh** and **5-Ir**[a]

	M=Rh1	M=Ir1		M=Rh1	M=Ir1
M–N1	2.0649(14)	2.067(10)	M–N2	1.9221(15)	1.856(10)
M–N3	2.0782(15)	2.068(10)	M–Cl1	2.3559(4)	2.357(4)
M–Cl2	2.4892(4)	2.465(4)	M–C10	2.0424(18)	1.997(12)
N1–C2	1.302(2)	1.278(14)	N3–C8	1.307(2)	1.287(15)
C2–C3	1.482(2)	1.508(16)	C7–C8	1.480(3)	1.510(17)
C10–Cl3	1.8141(18)	1.825(12)	N2···Cl3	3.0548(15)	3.070(10)
N1–M–N3	159.21(6)	158.9(4)	N2–M–Cl1	177.91(4)	177.3(3)
Cl2–M–C10	177.45(5)	178.0(4)	M–C10–Cl3	114.73(9)	117.5(7)
N1–M–N2	79.77(6)	79.3(4)	N1–M–Cl1	100.39(4)	100.4(3)
N2–M–N3	79.88(6)	79.8(4)	N3–M–Cl1	100.11(4)	100.6(3)

[a] Esd's in parentheses.

in complexes **5-Rh** and **5-Ir** (*cf.* below). The rhodium chlorido bond length of 2.3559(4) Å (Rh1–Cl1) within the plane of the terdentate N-donor is comparable to the corresponding distance in the rhodium(I) chlorido complex **2-Rh** (Rh1–Cl1, 2.3211(4)). It is notably shorter than the Rh–Cl bond (Rh1–Cl2, 2.4892(4) Å) to the apical chlorido ligand, which is attributed to the larger *trans* influence of the chloromethyl group. A similar alternation of the bond lengths in related octahedral pyridine, diimine complexes was previously reported by us and others for methyl bis-triflato Rh complexes.[15,16] Particularly noteworthy is the distortion from the ideal octahedral geometry, which becomes immediately apparent from inspection of the side view of complex **5-Rh** shown in Fig. 3 and which is also present in the iridium congener **5-Ir**. Similar deviations are found in related octahedral rhodium(III) complexes previously studied by us[16] and might be attributed to steric repulsion of the apical groups and the ligands in the equatorial plane.

Following a previously established route by our group,[4,16] the desired methoxido iridium precursor compound **3** was obtained from **2-Ir** by metathesis with sodium methoxide and was then further converted to the azido complex **4-Cl** by reaction with trimethylsilyl azide (Scheme 1). The constitutions of complexes **3** and **4-Cl** were confirmed by ^{1}H, ^{13}C, and IR spectroscopy, as well as elemental analysis for complex **3**. The IR spectrum of the azido complex **4-Cl** shows a strong absorption at 2035 cm^{-1}, which could be unambiguously assigned to the asymmetrical stretching vibration of the azido group by comparison of the IR spectrum of **4-Cl** with its single labeled ^{15}N-isotopologue, **4-Cl-^{15}N**, Ir-^{15}N═N$_2$ (Ir–N═N═^{15}N).

Thermoanalytical studies

The thermolyses of the 2,6-dichloro and 2,6-dimethyl aryl substituted azido complexes **4-Cl** and **4-Me** were studied by differential scanning calorimetry (DSC) and combined differential thermogravimetry/mass spectrometry (DTG-MS). The recorded DSC curves for complexes **4-Cl** and **4-Me** are presented in Fig. 4. The inspection of the DSC traces shown in Fig. 4 self-evidently reveals the disparities of the thermal properties of the chloro and methyl aryl substituted derivatives **4-Me** and **4-Cl**. While there is only *one* exothermic process notable for complex **4-Me**, there are *two* clearly separated exothermic steps in the DSC trace of the chloro aryl compound **4-Cl**. The DSC experiment of the 2,6-dimethyl aryl substituted azido complex **4-Me** revealed an exothermic peak at 112 °C with an enthalpy of –35.2 kcal mol^{-1}. The complementary DTG/MS experiment for **4-Me** evidenced a mass loss of 6.89% (calculated for N_2 loss: 4.64%) at this temperature with concurrent signals at m/z = 28 and 14 for N_2^+ and N_2^{2+} in the mass spectrometric trace of the volatiles. The observed experimental enthalpy of –35.2 kcal mol^{-1} for **4-Me** is considerably higher than the previously determined value of –6 kcal mol^{-1} for the formation of the (isolated) iridium nitrido complex from its azido precursor in the 2,6-diisopropyl phenyl substituted derivative.[4] For the conversion of the azido compound to the putative nitrido complex ([Ir]–N$_3$ → [Ir]≡N + N$_2$; **4-Me** → **6-Me**) values of –0.4, respectively –5.3 kcal mol^{-1} were calculated by DFT methods with the BP-86 and B3LYP functionals.

For the C–H activation step of one of the benzylic methyl groups (Scheme 2) by the putative nitrido complex **6-Me** a strongly

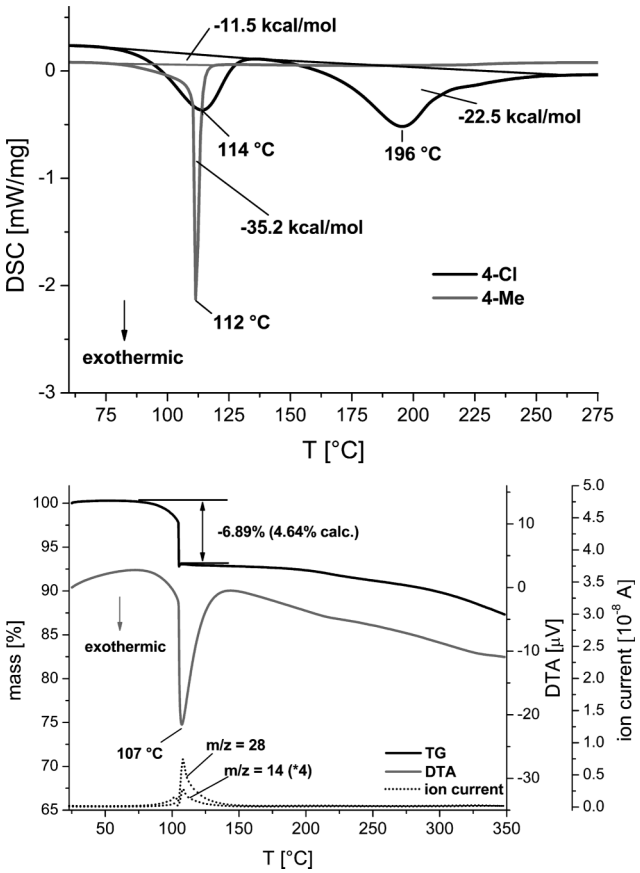

Fig. 4 Above: DSC traces for complexes **4-Me** (gray) and **4-Cl** (black); below: DTA and TG/MS curves for **4-Me** (black: TG, gray: DTA, dotted: mass traces).

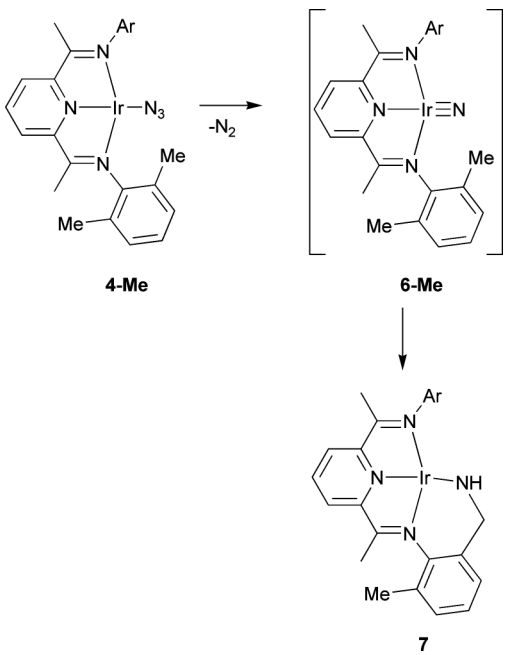

Scheme 2 Thermolysis of the azido complex **4-Me** and a potential product.

energetically favoured situation (–29.9(BP-86) and –29.3(B3LYP) kcal mol^{-1}) was estimated by DFT calculations. It

should be noted that an experimental value of $\Delta H = -21$ kcal mol^{-1} was previously established for C–H activation of the benzylic C–H bond in the corresponding 2,6-diisopropyl substituted derivative in DSC measurements.[11] These combined experimental and theoretical findings indicate that the extrusion of dinitrogen and the tentative subsequent C–H activation step ("tuck-in"-formation) are *not* kinetically separated for the methyl substituted azido complex **4-Me** (Scheme 2). Attempts to fully characterize the final thermolysis product(s) were so far unsuccessful. The ^{1}H NMR spectrum of a sample in THF-d_8 recorded at RT revealed a large number of peaks, which could not be unambiguously assigned, suggesting the presence of several products rather than a single product. The ^{1}H NMR spectra recorded at −80 °C of a sample prepared at low temperatures by condensation of THF-d_8 to the solid thermolyzed residue of **4-Me** at −196 °C showed prominent broad down-field shifted peaks at $\delta = 25.5$ and 16.8 ppm besides further signals in the range from 0–10 ppm (see ESI†). Most notably, we did not detect peaks in the anticipated high-field range of −10 to −40 ppm, indicative of hydride ligands. The broad resonances at $\delta = 25.5$ and 16.8 ppm disappeared upon allowing the sample to warm up to RT, giving the aforementioned ^{1}H NMR spectrum of a sample prepared at RT. Although, we can only speculate on the identity of the thermolyzed material, based on the resonances $\delta = 25.5$ and 16.8 ppm, we suspect that a paramagnetic intermediate is among it, which converts further at RT.

The inspection of the DSC curve for the chloro substituted azido complex **4-Cl** revealed an entirely different picture. In contrast to the results for complex **4-Me**, two well separated signals with maxima at 114 and 196 °C were detected in the temperature range from 70–270 °C. Based on the recorded mass loss of 4.63% (calculated: 4.09%) and a concomitant signature of 28 m/z (N_2^+) of the volatiles, initiated at 70 °C in the DTG-MS analysis (Fig. 5), the first step is assigned to the release of dinitrogen from the azido complex **4-Cl** giving the corresponding nitrido compound **6-Cl**.

The signal integrates to an enthalpy of −11.5 kcal mol^{-1}, which is in the range derived for the isolated iridium nitrido complex with 2,6-diisopropyl phenyl groups.[4] The signal for dinitrogen release passes on to the second exothermic peak, which has a maximum at

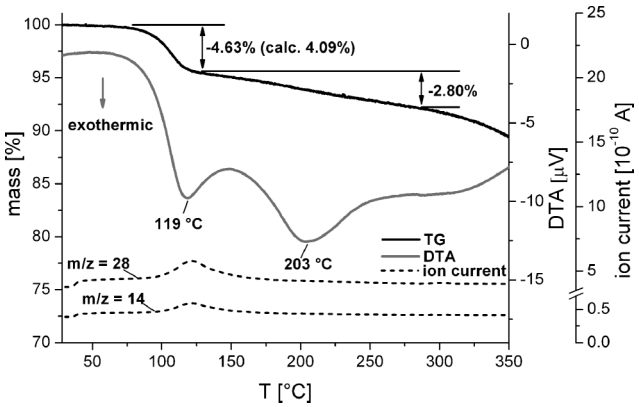

Fig. 5 DTA and TG/MS curves for **4-Cl** (black: TG, gray: DTA, dotted: mass traces).

196 °C with an integrated enthalpy of −22.5 kcal mol^{-1}. DTG-MS analysis for this step revealed a mass loss of 2.8%, but elemental analysis of the product obtained by batch thermolysis at 150 °C for 19 h showed no significant deviation from the product obtained from thermolysis at 90 °C, suggesting decomposition setting in above 200 °C (*cf.* ref. 11).

The product obtained in the second step of the DSC measurement by heating **4-Cl** over 150 °C proved to be rather insoluble in all tested organic solvents thus thwarting further NMR characterization. Since the IR and UV/vis spectra recorded as KBr pellets were not instructive, we can only speculate on the product(s). DFT calculations were performed for the two potential products **8a** and **8b** obtained by activation of the aryl C–Cl bond (Scheme 3), which are both energetically downhill from **6-Cl**. As anticipated, the formation of the less likely amido N–Cl compound **8a** is significantly less favoured than the corresponding chlorido, imido complex **8b** (**6-Cl** → **8a**: −18 kcal mol^{-1}; **6-Cl** → **8b**: −32 kcal mol^{-1}). The transition state for C–Cl activation could be located in the DFT calculations and is presented in Fig. 6. The corresponding barrier of 28 kcal mol^{-1} for this process is consistent with a set-in temperature of 150 °C observed in the DSC measurements. Based on the analysis of the frontier orbitals

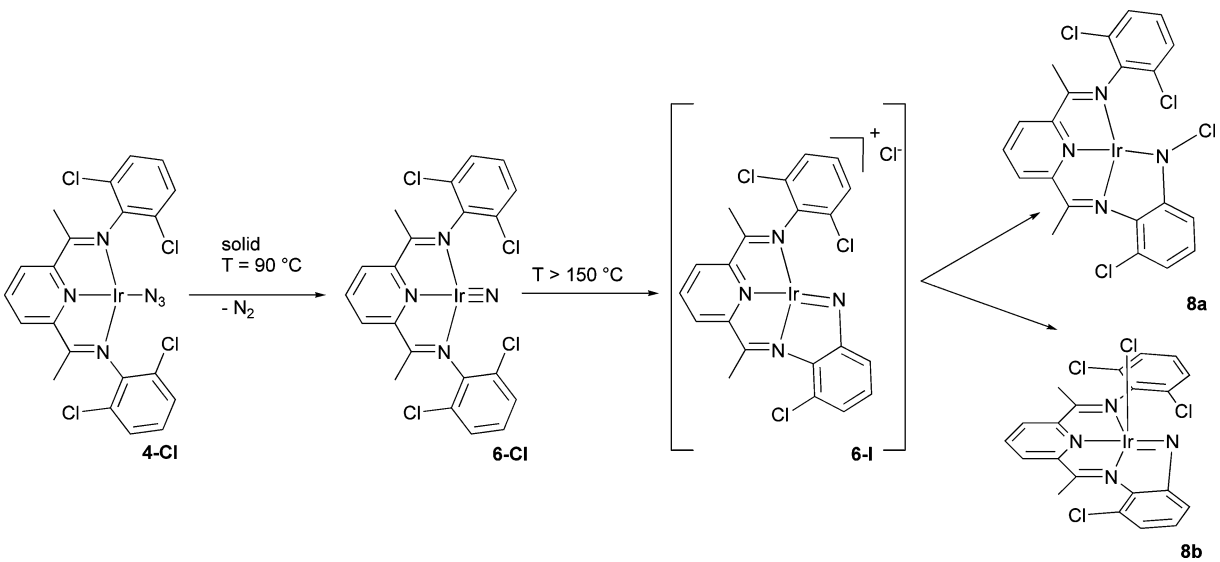

Scheme 3 Thermolysis of the azido complex **4-Cl**.

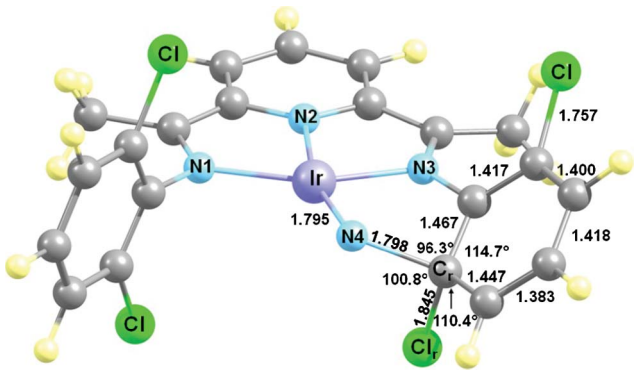

Fig. 6 Transition state for intramolecular C–Cl activation with selected distances and angles in [Å] and [°].

and considering the rather electron-deficient nature of the 2,6-dichloro substituted aryl group, it is deemed that this step proceeds by nucleophilic attack of the nitrido group at the aromatic carbon atom. At first glance, inspection of Fig. 6 might suggest formation of a Meisenheimer intermediate with close resemblance to the transition state structure. However, the IRC calculations provided strong arguments against this view and showed that the reaction mode proceeds in fact by release of a chloride ion to give an intermediate **6-I** in the product direction (Scheme 3).

The Fukui function for nucleophilic attack f^+ of **6-I** presented in Fig. 7 revealed two preferential sites for addition of the chloride ion in a consecutive step. The preferential sites for nucleophilic attack are a) the nitrogen atom of the former nitrido unit and b) the iridium center, which would lead to either **8a** and **8b** upon addition of the chloride ion. As noted above, the DFT calculations showed that the iridium(III) complex **8b** is 14 kcal mol^{-1} more stable than the Ir(I) compound **8a**.

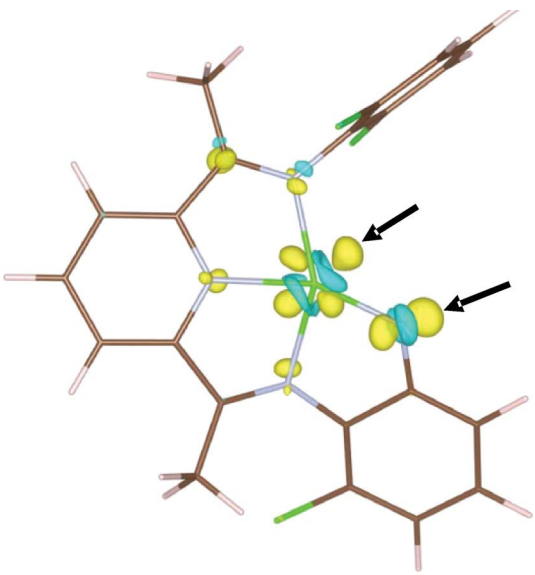

Fig. 7 Fukui f^+ function for the nucleophilic attack in **6-I**. The arrows indicate sites for preferential attack.

In order to optimize the conditions for the preparation of the tentative nitrido complex **6-Cl**, DSC measurements of the azido complex **4-Cl** were performed in cyclic mode between 50 and 90 °C (Fig. 8).

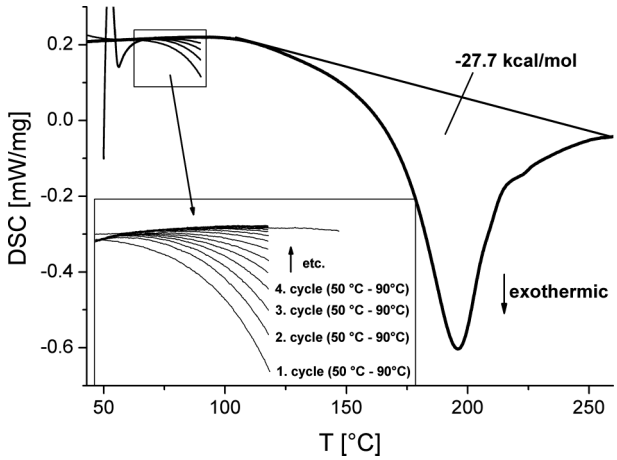

Fig. 8 DSC measurement of the azido complex **4-Cl** in cyclic mode between 50–90 °C and between 0–350 °C after complete N_2 extrusion.

As shown in Fig. 8, thermolysis of complex **4-Cl** at 90 °C yields only the product of the N_2 release, suppressing the second thermal step.

Characterization of the thermolysis product 6-Cl

The compound obtained by the reaction of the azido complex **4-Cl** at 90 °C was sparingly soluble in all tested organic solvents, thwarting NMR measurements in solution.[17] The elemental analysis of the thermolyzed product was consistent with N_2 loss, which was further supported through the absence of an azido stretching vibration in the range of 2030 cm^{-1} in the IR spectrum. Furthermore, a new IR band was detected at 955 cm^{-1}, which red-shifted by *ca.* 30 cm^{-1} for the thermolyzed ^{15}N labeled isotopologue of **4-Cl-^{15}N** (Fig. 9). Together with the good agreement of the ν(Ir≡N) stretching frequency of the aforementioned isolated terminal Ir nitrido complex with 2,6-diisopropyl phenyl groups, **6-iPr** located at 958 cm^{-1},[4] we assigned this band to a ν(Ir≡N) vibration.

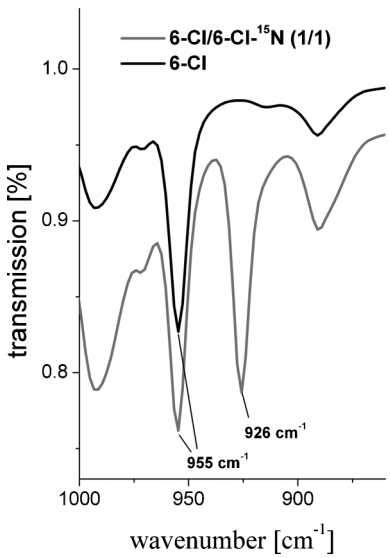

Fig. 9 Section of the IR spectra (KBr) of the nitrido complexes **6-Cl** (black) and **6-Cl-^{15}N** (gray).

The solid state UV/vis spectrum measured as KBr pellet is also comparable to the structural characterized Ir nitrido complex **6-iPr**, exhibiting a strong maximum at 593 nm in the visible range with two further broad maxima at 766 and 830 nm in the near infrared. Based on this combined analytical data, assignment of the thermolyzed material to the terminal nitrido complex **6-Cl** seemed justified.

Further, compelling evidence was provided by reaction of **6-Cl** with silanes. Although the thermolyzed material **6-Cl** is almost insoluble in organic solvents, addition of a THF or toluene solution of either triethyl- or triphenylsilane to a solid sample of **6-Cl**, resulted in a quick dissolution of most of the solid material to give brown/green colored solutions (Scheme 4).

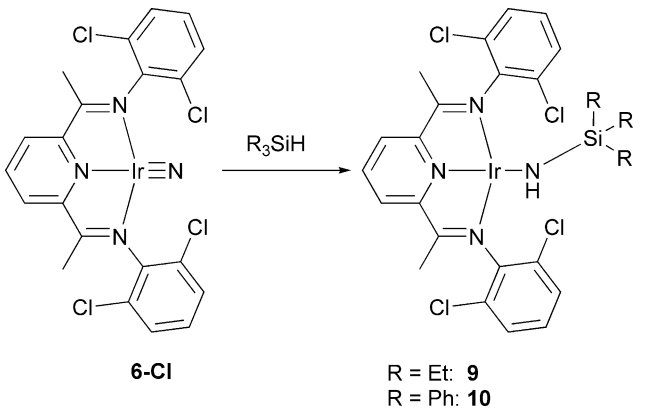

Scheme 4 Reaction of the nitrido complex **6-Cl** with silanes.

Inspection of the ^{1}H NMR spectra of the products **9** and **10** obtained from reaction of **6-Cl** with triethyl- or triphenylsilane revealed the formation of C_{2v}-symmetrical complexes, indicated by singlets for the ketimine methyl groups and doublets and triplets in 2 : 1 integration ratio for the meta and para pyridine protons. Mostly diagnostical was the observation of broad singlets at δ = 8.06 (Et_3SiH; C_6D_6) and 7.22 (Ph_3SiH; THF-d_8) ppm, which were assigned to amido protons based on ^{1}H-^{15}N correlated NMR spectroscopy (HSQC). Compared to the estimated yields of up to 50% and up to 90% for **9** and **10** derived from NMR tube reactions of **6-Cl** with the silanes by integration of appropriate ^{1}H NMR signals against the resonance of ferrocene used as internal standard (*cf.* ESI†), the isolated yields are significantly diminished. In fact only the triphenyl silylamido complex **10** could be obtained in 8% yield as a reasonably pure product, which was further characterized by ^{13}C NMR spectroscopy. For complex **10**, we also obtained single crystals suitable for X-ray structure analysis, which allowed to establish the anticipated amido structure. The molecular structure of complex **10** is given in Fig. 10, selected bond lengths and angles are given in Table 3.

The sum of angles of 360.1° around the iridium center revealed a pseudo square-planar geometry. In comparison with the rhodium chlorido complex **2-Rh** the ketimine C–N bonds are slightly longer (N1–C2: 1.350(9) Å, N3–C8: 1.336(9) Å), while the exocylic C–C bonds to the pyridine ring are shorter (C2–C3: 1.416(11), C7–C8: 1.431(10)). This is indicative of more electron transfer to the pyridine, diimine ligand system, which is consistent with the strong π-donor propensity of the amido group. The most prominent

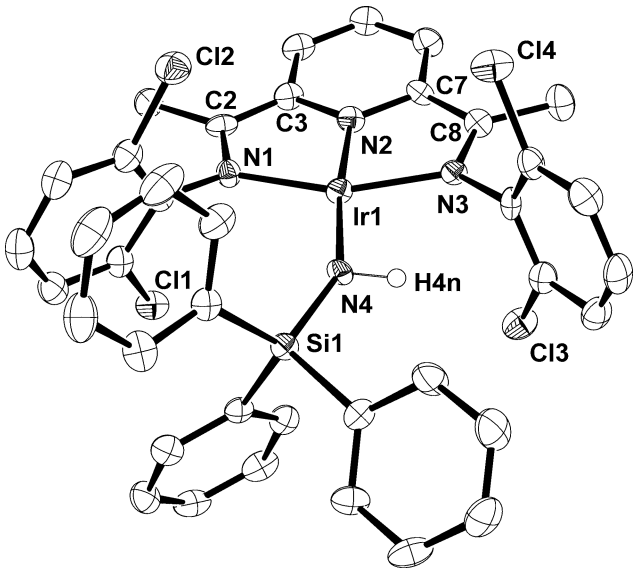

Fig. 10 Ortep representation of complex **10** with anisotropic displacement parameters shown at the 50% probability level. Hydrogen atoms and a co-crystallized Et_2O molecule are omitted for clarity.

Table 3 Selected bond lengths (Å) and angles (°) of **10**[a]

Ir1–N1	2.042(6)	Ir1–N2	1.911(6)
Ir1–N3	2.006(6)	Ir1–N4	1.998(5)
N4–H4n	0.95(12)	N4–Si1	1.694(6)
N1–C2	1.350(9)	N3–C8	1.336(9)
C2–C3	1.416(11)	C7–C8	1.431(10)
N1–Ir1–N3	157.2(2)	N2–Ir1–N4	173.4(3)
N1–Ir1–N2	78.7(2)	N1–Ir1–N4	107.9(2)
N2–Ir1–N3	78.8(2)	N3–Ir1–N4	94.7(2)
Ir1–N4–Si1	144.5(4)		

[a] Esd's in parentheses.

structural feature is the bonding situation of the amido nitrogen atom N4. While the Ir1–N4 bond length of 1.998(5) Å is in the expected range, it displays a short N–Si bond of 1.694(6) Å. It is also bonded to hydrogen atom H4n, which was located in the difference Fourier map and was isotropically refined. The sum angles around N4 of 357.5° and the position of atom Si1 within the plane of the terdentate ligand framework and the iridium center suggests sp^2-hybridzation of the amido nitrogen atom N4. Mostly noticeable are the large Ir1–N4–Si1 angle of 144.5° and the asymmetrical bonding angles N4–Ir1–N1 (107.9(2)°) and N4–Ir1–N3 (94.7(2)°) between the ketimine (N1,N3) and amido nitrogen atoms. The larger value of the latter two angles is found on the side of the bulky triphenylsilane group suggesting that steric repulsion is responsible for widening up both the Ir1–N4–Si1 and N4–Ir1–N1 angles. This view is supported by DFT calculations of the hydrogen substituted model complex shown below (Ar = 2,6-$C_6H_3Cl_2$), bond lengths and angles in (Å) and (°)) and the DFT optimized geometry of the full structure, which revealed a smaller Ir–N_{amido}–Si angle of 130.3°.

Since the idealized molecular structure observed in the solid state corresponds to C_s-symmetry, the C_{2v}-symmetrical signature in the ^{1}H NMR spectrum of **10** at RT suggests a fast site

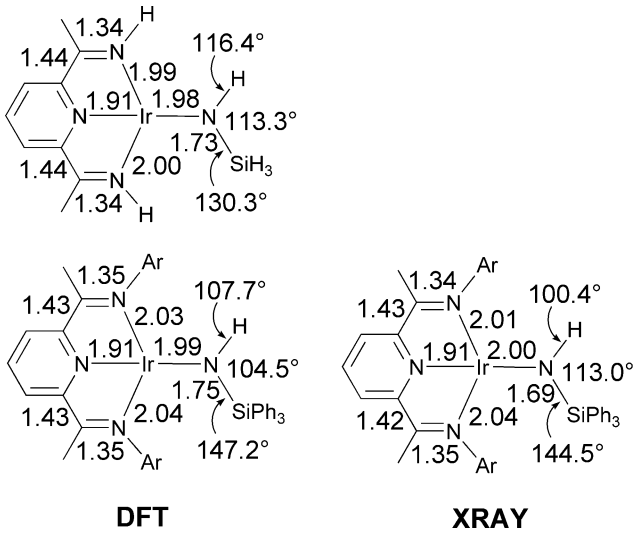

DFT **XRAY**

exchange of the $SiPh_3$ group and the amido hydrogen atom on the NMR time scale. When a sample of complex **10** was cooled to –100 °C, significant changes of the ^1H NMR spectrum were indeed noticed. For the resonances of the meta hydrogen atoms of the pyridine ring, the singlet for the ketimine methyl groups as well as all aromatic resonances a significant broadening was now observed, suggesting loss of the mirror plane perpendicular to the N_3 ligand framework. This is consistent with the C_s-symmetrical structure observed in the solid state. Unfortunately, with coalescence expected slightly below –100 °C, we were not able to perform a lineshape NMR analysis.

We analyzed this process by DFT methods and located the transition state presented in Fig. 11. The transition state also displays idealized C_s-symmetry, the mirror plane is now however perpendicular to the plane spanned by the pyridine, diimine donor plane and contains the hydrogen and Si atom of the amido ligand. The calculated barrier amounts to 15 kcal mol^{-1}, which is in the range anticipated for fluctional processes detectable by ^1H NMR spectroscopy. The barrier can be rationalized by loss of a stabilizing push pull interaction ($4e^-$ 3 orbital) in the transition state between (i) the lone pair (p_z) of the sp^2-hybridized amido π-donor atom N4, (ii) the occupied d_{xz} orbital of the iridium center and (iii) an acceptor orbital located on the pyridine part of the terdentate ligand. This type of stabilization was previously discussed by us for the corresponding methoxido complexes, for which a slightly smaller barrier of 12 kcal mol^{-1} was calculated.[16] It deserves a special mention that IRC-calculations for this process show that it requires only little movement of the triphenylsilyl group while the hydrogen atom H4 is essentially responsible for the left-right site exchange.

Experimental

General

All manipulations of the complexes were performed under standard Schlenk techniques or in a dinitrogen filled glovebox. Pentane, benzene, toluene, diethylether (Et_2O) and tetrahydrofuran (THF) were distilled over sodium benzophenone ketyl prior to use. CH_2Cl_2 was distilled over P_2O_5 followed by CaH_2, MeOH was distilled over Mg prior to use. Trimethylsilyl azide was purchased from Merck or Aldrich and was vacuum transferred prior to use. Isotopically labelled NaN_3 (terminal ^{15}N, 98%) for the preparation of $Me_3Si^{15}NN_2/N_2{}^{15}N$ was used as purchased from Cambridge Isotope Laboratories. All other reagents were purchased from commercial sources and were used as received. The dimeric Ir[18] and Rh[19] precursors $[M(C_2H_4)_2Cl]_2$ and the methoxido complex $[Ir(Me_4N_3)OMe]$[16] were prepared as described in literature. ^1H, ^{13}C, ^{15}N and ^{29}Si NMR spectra were recorded on Bruker Avance 400, Bruker DRX 500 and Varian Gemini 2000 BB NMR spectrometers. The ^1H and ^{13}C NMR spectra are referenced to the residual resonances of the solvent. The ^{15}N NMR shifts are referenced to NH_3, the internal standard of the instrument ($\delta(NH_3)_{(l)}$ = –380 ppm *vs.* $MeNO_{2(l)}$). The ^{29}Si NMR shifts are referenced to Me_4Si. The assignments of the ^{13}C NMR spectra were carried out by combined analyses of DEPT and ^{13}C–^1H correlated spectra (HSQC and HMBC). The UV/vis spectra were recorded on a Cary 50 spectrometer in 1 cm quartz cuvettes or as KBr pellets. Elemental analyses were measured by: Zentrale Elementaranalyse, Universität Hamburg. IR spectra were measured on a Bruker Vertex 70 IR spectrometer. DSC measurements were performed on a Netzsch DSC 204 F1 with a heating rate of 10 K min^{-1} in broached aluminium pans in a nitrogen atmosphere. The instrument was calibrated against the melting enthalpy of indium. DTA/TG-MS measurements were recorded on a Netzsch STA/TG 409C/CD coupled with a Balzer MID quadrupole mass

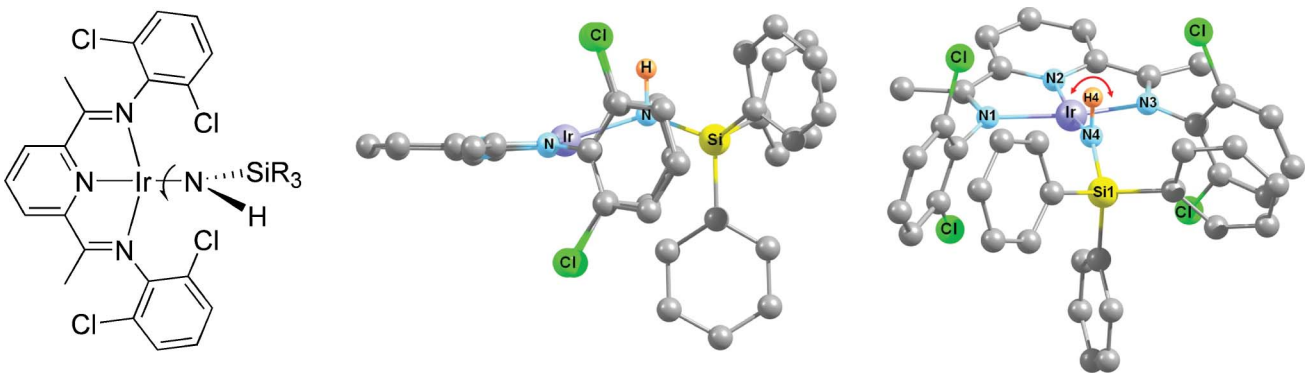

Fig. 11 Schematic, side and front view of the transition state for the left-right site exchange. Selected distances [Å] and angles [°]: Ir–N4: 2.06, Ir–N2: 1.92., N4–Si1: 1.71, N2–Ir–N4: 170.3, N1–Ir–N4: 101.8, N3–Ir–N4: 100.2, Ir–N4–H4: 105.4, Ir–N4–Si1: 142.9, H4–N4–Si1:111.7.

spectrometer or a Netzsch STA/TG 449F3 coupled with a Netzsch QMS 403 C Aëolos quadrupole mass spectrometer with a heating rate of 10 K min^{-1} in an argon atmosphere.

X-ray crystallography

Crystals of **1**, **2-Rh**, **5-Ir**, **5-Rh** and **10** suitable for X-ray structural determinations were mounted in polybutene oil on a glass fibre and transferred on the goniometer head to the precooled instrument. Crystallographic measurements were carried out with Mo Kα radiation from a Incoatec Microfocus source on a Bruker APEX single crystal diffractometer operating at 100(2) K. The structures were solved by direct methods and refined against F^2 by full matrix least squares (SHELX97)[20] using all unique data. All non-hydrogen atoms were anisotropically refined unless otherwise reported; the carbon bound hydrogen atoms were placed in geometrically calculated positions and refined using a riding model. Molecular graphics were prepared using ORTEP3.[21] The asymmetric unit of complex **2-Rh** contains one co-crystallized THF molecule. The thermal ellipsoid of the THF oxygen atom suggests a small degree of disorder. The asymmetric unit of complex **5-Ir** contains one co-crystallized CH_2Cl_2 molecule. After anisotropical refinement, several atoms (N1–N3, C2, C3, C7, C8, C10, C12, C16, C17, C20) were non-positive definite, which is assumed to be due to the low overall quality of the collected data. ISOR was used to adjust the atomic displacements to realistic values (0.008: C2, C3, C7, C12, C16; 0.007: C8, C17; 0.005: C10; 0.004: N1–N3). The asymmetric unit of complex **5-Rh** contains one co-crystallized CH_2Cl_2 molecule. The asymmetric unit of complex **10** contains one co-crystallized diethylether molecule. After anisotropical refinement the amido nitrogen atom (N4) was non-positive definite. Refinement as a nitrogen atom seems justified, since complex **10** is neutral and diamagnetic and displays $^1J(^1H\text{-}^{15}N)$ coupling in the aforementioned HSQC experiment. ISOR (0.0015) was used to adjust the atomic displacements to realistic values. The amido hydrogen atom (H4n) could be located in the Fourier electron density maps and was refined freely with isotropic displacement parameters. Further details of the data collection and processing are given in Table 4 and in the supplemental CIF files†.

Syntheses

Synthesis of the ligand (Cl_4N_3) (1). A 250 ml round bottom flask, equipped with a dean stark trap and a reflux condenser was charged with 6.54 g (40.1 mmol) 2,6-diacetylpyridine and 15.0 g (92.6 mmol) 2,6-dichloroaniline. 175 ml of dry benzene and a spatula point (~20 mg) of *p*-toluenesulfonic acid monohydrate were added and the atmosphere was changed to nitrogen by three evacuation/refill cycles. The reaction solution was then refluxed for 17 h under nitrogen, whereas the colour of the solution changed to brown-yellow. The solvent was removed under reduced pressure and the resulting brown oil was dissolved in 400 ml of Et_2O, which was then extracted with three portions of 100 ml distilled H_2O. The Et_2O phase was dried over sodium sulphate, filtrated and removed under reduced pressure. The residue was dried in vacuum. Addition of 20 ml of methanol resulted in a beige solid, which was collected by filtration, washed four times with 10 ml methanol and dried in vacuum. Recrystallization from refluxing acetone afforded 3.4 g of pale yellow crystals (suitable for single crystal X-ray diffraction), which were washed with two portions of 10 ml acetone and dried in vacuum. More product can be obtained by successive recrystallization from the mother liquor giving a combined yield of 5.20 g (11.5 mmol, 29%). ^{1}H NMR (400 MHz, CD_2Cl_2): δ = 8.51 (d, 2H, ^3J = 7.8 Hz, $C_{py}\boldsymbol{H}(3,5)$); 7.99 (t, 1H, ^3J = 7.8 Hz, $C_{py}\boldsymbol{H}(4)$); 7.40 (d, 4H, ^3J = 8.1 Hz, $C_{arom}\boldsymbol{H}(3,5)$); 7.04 (t, 2H, ^3J = 8.1 Hz, $C_{arom}\boldsymbol{H}(4)$); 2.36 (s, 6H, NC-C$\boldsymbol{H}_3$) ppm. ^{13}C{1H} NMR (100 MHz, CD_2Cl_2): δ = 171.8 ($\boldsymbol{C}$=N); 155.0 ($\boldsymbol{C}_{py}(2,6)$); 146.2 ($\boldsymbol{C}_{arom}(1)$); 137.9 ($\boldsymbol{C}_{py}(4)$); 128.8 ($\boldsymbol{C}_{arom}(3,5)$); 125.0 ($\boldsymbol{C}_{arom}(4)$); 124.7 ($\boldsymbol{C}_{arom}(2,6)$); 124.0 ($\boldsymbol{C}_{py}(3,5)$); 17.9 (NC-$\boldsymbol{C}H_3$) ppm. Anal. calcd. for $C_{21}H_{15}Cl_4N_3$: C, 55.90; H, 3.35; N, 9.31. Found: C, 56.00; H, 3.44; N, 9.3.

Synthesis of [Ir(Cl_4N_3)Cl] (2-Ir). In a 100 ml round-bottomed Schlenk flask 2.12 g (4.69 mmol) of the ligand (Cl_4N_3) (**1**) was dissolved in 15 ml of THF under N_2. This solution was then

Table 4 Crystallographic data

Compound reference	**1**	**2-Rh·THF**	**5-Rh·CH_2Cl_2**	**5-Ir·CH_2Cl_2**	**10·Et_2O**
Chemical formula	$C_{21}H_{15}Cl_4N_3$	$C_{25}H_{23}Cl_5N_3ORh$	$C_{23}H_{19}Cl_9N_3Rh$	$C_{23}H_{19}Cl_9IrN_3$	$C_{43}H_{41}Cl_4IrN_4OSi$
Formula mass	451.16	661.62	759.37	848.66	991.58
Crystal system	Monoclinic	Monoclinic	Monoclinic	Monoclinic	Triclinic
a/Å	9.3466(5)	9.7883(2)	11.5360(2)	11.557(9)	10.8214(5)
b/Å	14.2468(7)	10.4967(2)	19.3875(4)	19.363(15)	12.3189(5)
c/Å	15.4849(8)	26.4832(5)	13.7023(3)	13.696(11)	15.9789(7)
α/°	90.00	90.00	90.00	90.00	81.104(2)
β/°	99.4560(10)	98.0900(10)	106.1570(10)	105.860(13)	78.966(2)
γ/°	90.00	90.00	90.00	90.00	86.105(3)
Unit cell volume/Å^3	2033.94(18)	2693.93(9)	2943.53(10)	2948(4)	2063.97(16)
Temperature/K	100(2)	100(2)	100(2)	103(2)	100(2)
Space group	$P2_1/n$	$P2_1/n$	$P2_1/n$	$P2_1/n$	$P\bar{1}$
No. of formula units per unit cell, *Z*	4	4	4	4	2
No. of reflections measured	49083	50469	59216	15898	23008
No. of independent reflections	5901	6193	10337	5183	8803
R_{int}	0.0558	0.0252	0.0386	0.1327	0.0458
Final R_1 values ($I > 2\sigma(I)$)	0.0352	0.0221	0.0310	0.0553	0.0517
Final $wR(F^2)$ values ($I > 2\sigma(I)$)	0.0822	0.0512	0.0593	0.0870	0.1288
Final R_1 values (all data)	0.0520	0.0249	0.0488	0.1217	0.0626
Final $wR(F^2)$ values (all data)	0.0873	0.0534	0.0658	0.0999	0.1354
Goodness of fit on F^2	0.972	1.049	1.043	0.715	1.160

treated with a red solution of 1.20 g (2.11 mmol) $[Ir(C_2H_4)_2Cl]_2$ in 30 ml Et_2O, which resulted in an immediate colour change to dark green. The solution was stirred for an additional hour, whereas the green product precipitated from the solution. The solvent was removed in vacuum and the dried raw product was washed in ~10 ml portions of a total of 60 ml of a THF/Et_2O mixture (1/1) and 5 ml of pentane. After drying the residue for several hours in vacuum, the analytically pure product was obtained in 42% yield (1.35 g; 1.99 mmol). ^{1}H NMR (400 MHz, CD_2Cl_2): δ = 8.87 (t, 1H, ^3J = 8.0 Hz, $C_{py}\boldsymbol{H}(4)$); 8.09 (d, 2H, ^3J = 8.0 Hz, $C_{py}\boldsymbol{H}(3,5)$); 7.53 (d, 4H, ^3J = 8.3 Hz, $C_{arom}\boldsymbol{H}(3,5)$); 7.27 (t, 2H, ^3J = 8.1 Hz, $C_{arom}\boldsymbol{H}(4)$); 0.87 (s, 6H, NC-C$\boldsymbol{H}_3$) ppm. ^{13}C{1H} NMR (100 MHz, CD_2Cl_2): δ = 176.6 ($\boldsymbol{C}$=N); 164.1 ($\boldsymbol{C}_{py}(2,6)$); 149 ($\boldsymbol{C}_{arom}(1)$); 129.5 ($\boldsymbol{C}_{arom}(2,6)$); 128.7 ($\boldsymbol{C}_{arom}(3,5)$); 128.4 ($\boldsymbol{C}_{arom}(4)$); 125.2 ($\boldsymbol{C}_{py}(3,5)$); 124.3 ($\boldsymbol{C}_{py}(4)$); 20.6 (NC-$\boldsymbol{C}H_3$) ppm. IR (KBr): ν_{max} [cm^{-1}] = 3085, 1934, 1563, 1485, 1436(s), 1411, 1375, 1327, 1294, 1233, 1148, 790(m), 773, 729, 680. Anal. calcd. for $C_{21}H_{15}Cl_5IrN_3$: C, 37.15; H, 2.23; N, 6.19. Found: C, 36.76; H, 2.35; N, 6.00.

Synthesis of [Rh(Cl$_4$N$_3$)Cl] (2-Rh). A solution of 179 mg (0.460 mmol) of the dimeric complex $[Rh(C_2H_4)_2Cl]_2$ in 8 ml of toluene was added dropwise to a stirred solution of 400 mg (0.887 mmol) of ligand **1** in 11 ml of toluene. The solution was stirred for 11 h, whereas the green product precipitated from the solution. The solution was decanted from the solid residue, which was then washed with three portions of 5 ml THF/Et_2O (1/2) and dried in vacuum. 499 mg (0.846 mmol; 95%) of the green complex [Rh(Cl$_4$N$_3$)Cl] (**2-Rh**) were obtained. Single crystals suitable for X-ray diffraction analysis were obtained from a concentrated THF solution layered with hexane at –35 °C. ^{1}H NMR (400 MHz, CD_2Cl_2): δ = 8.59 (t, 1H, ^3J = 8.0 Hz, $C_{py}\boldsymbol{H}(4)$); 7.83 (d, 2H, ^3J = 8.0 Hz, $C_{py}\boldsymbol{H}(3,5)$); 7.47 (m, 4H, $C_{arom}\boldsymbol{H}(3,5)$); 7.27 (m, 2H, $C_{arom}\boldsymbol{H}(4)$); 1.60 (s, 6H, NC-C$\boldsymbol{H}_3$) ppm. ^{13}C{1H} NMR (100 MHz, CD_2Cl_2): δ = 171 ($\boldsymbol{C}$=N); 156.5 ($\boldsymbol{C}_{py}(2,6)$); 146.0 ($\boldsymbol{C}_{arom}(1)$); 129.1 ($\boldsymbol{C}_{arom}(2,6)$); 128.9 ($\boldsymbol{C}_{arom}(3,5)$); 127.8 ($\boldsymbol{C}_{arom}(4)$); 127.1 ($\boldsymbol{C}_{py}(3,5)$); 125.0 ($\boldsymbol{C}_{py}(4)$); 18 (NC-$\boldsymbol{C}H_3$) ppm. Anal. calcd. for $C_{21}H_{15}Cl_5N_3Rh$: C, 42.78; H, 2.56; N, 7.13. Found: C, 42.89; H, 2.64; N, 6.93.

Synthesis of [Ir(Cl$_4$N$_3$)(Cl)$_2$(CH$_2$Cl)] (5-Ir). A solution of 70 mg (100 µmol) of the complex [Ir(Cl$_4$N$_3$)Cl] (**2-Ir**) in 15 ml CH_2Cl_2 was placed in a J. Young teflon valve tapped Schlenk tube. While stirred, the solution was heated at 55 °C for 63 h, upon which the color of the solution changed to orange. The solution was allowed to cool to room temperature, which gave single crystals suitable for X-ray diffraction. The solvent was removed in vacuum and the residue was washed in portions with 15 ml of pentane. After five hours drying in vacuum, the analytically pure orange product was obtained in 95% yield (72 mg, 94 µmol). Because of the very low solubility of **5-Ir**, ^{13}C NMR spectroscopic characterization was not attempted. ^{1}H NMR (400 MHz, CD_2Cl_2): δ = 8.03–7.95 (m, 3H, $C_{py}\boldsymbol{H}(3,4,5)$); 7.50 (dd, 2H, ^3J = 8.1 Hz, ^4J = 1.4 Hz, $C_{arom}\boldsymbol{H}(5)$); 7.46 (dd, 2H, ^3J = 8.2 Hz, ^4J = 1.4 Hz, $C_{arom}\boldsymbol{H}(3)$); 7.29 (dd, 2H, ^3J = 8.2 Hz, ^3J = 8.2 Hz, $C_{arom}\boldsymbol{H}(4)$); 4.14 (s, 2H, C$\boldsymbol{H}_2$Cl); 2.98 (s, 6H, NC-C$\boldsymbol{H}_3$) ppm. Anal. calcd. for $C_{22}H_{17}Cl_7IrN_3$: C, 34.60; H, 2.24; N, 5.50. Found: C, 34.46; H, 2.42; N, 5.19.

Synthesis of [Rh(Cl$_4$N$_3$)(Cl)$_2$(CH$_2$Cl)] (5-Rh). 48 mg (81 µmol) **2-Rh** were dissolved in CH_2Cl_2 and stirred for 24 h at room temperature. The solution was then transferred to a Schlenk tube which was sealed with a J. Young teflon valve. While stirred, the solution was heated at 55 °C for 16 h. The solvent was removed in vacuum and residual solvents were co-evaporated with 3 ml pentane. After drying in vacuum, 48 mg (71 µmol; 88%) of the orange complex **5-Rh** were obtained. Single crystals suitable for X-ray diffraction analysis were obtained from a saturated solution of complex **2-Rh** in CH_2Cl_2 after several days at room temperature. Because of the very low solubility of **5-Rh**, ^{13}C NMR spectroscopic characterization was not attempted. ^{1}H NMR (400 MHz, CD_2Cl_2): δ = 8.32 (m, 1H, $C_{py}\boldsymbol{H}(4)$); 8.15 (m, 2H, $C_{py}\boldsymbol{H}(3,5)$); 7.47 (dd, 2H, ^3J = 8.0 Hz, ^4J = 1.4 Hz, $C_{arom}\boldsymbol{H}(5)$); 7.44 (dd, 2H, ^3J = 8.1 Hz, ^4J = 1.4 Hz, $C_{arom}\boldsymbol{H}(3)$); 7.29 (dd, 2H, ^3J = 8.1 Hz, ^3J = 8.1 Hz, $C_{arom}\boldsymbol{H}(4)$); 4.43 (d, 2H, $^2J_{Rh,H}$ = 3.2 Hz, C$\boldsymbol{H}_2$Cl); 2.63 (s, 6H, NC-C$\boldsymbol{H}_3$) ppm. Anal. calcd. for $C_{22}H_{17}Cl_7RhN_3$: C, 39.18; H, 2.54; N, 6.23. Found: C, 38.94; H, 2.61; N, 5.99.

Synthesis of [Ir(Cl$_4$N$_3$)OMe] (3). A 250 ml round bottom flask was charged with 744 mg (1.10 mmol) of the complex [Ir(Cl$_4$N$_3$)Cl] (**2-Ir**) and 179 mg (3.31 mmol) sodium methoxide. 15 ml THF and 120 ml of methanol were added and the suspension was stirred for 16 h. The solvents were removed in vacuum and the residue was dried for six hours in vacuum. Residual solvents were co-evaporated with two portions of 10 ml pentane each. After additional nine hours of drying in vacuum, the product was extracted from the residue into toluene. The toluene phase was removed in vacuum, which gave 640 mg of the green complex **3** (0.95 mmol, 86%). ^{1}H NMR (400 MHz, THF-d_8): δ = 8.61 (d, 2H, ^3J = 7.9 Hz, $C_{py}\boldsymbol{H}(3,5)$); 8.27 (t, 1H, ^3J = 7.9 Hz, $C_{py}\boldsymbol{H}(4)$); 7.47 (d, 4H, ^3J = 8.1 Hz, $C_{arom}\boldsymbol{H}(3,5)$); 7.27 (t, 2H, ^3J = 8.1 Hz, $C_{arom}\boldsymbol{H}(4)$); 5.06 (s, 3H, O-C$\boldsymbol{H}_3$); 0.54 (s, 6H, NC-C$\boldsymbol{H}_3$) ppm. ^{13}C{1H} NMR (100 MHz, THF-d_8): δ = 167.4 ($\boldsymbol{C}$=N); 161.3 ($\boldsymbol{C}_{py}(2,6)$); 152.4 ($\boldsymbol{C}_{arom}(1)$); 130.4 ($\boldsymbol{C}_{arom}(2,6)$); 129.2 ($\boldsymbol{C}_{arom}(3,5)$); 128.4 ($\boldsymbol{C}_{arom}(4)$); 124.4 ($\boldsymbol{C}_{py}(3,5)$); 117.6 ($\boldsymbol{C}_{py}(4)$); 68.0 (O-$\boldsymbol{C}H_3$); 21.0 (NC-$\boldsymbol{C}H_3$) ppm. IR (KBr): ν_{max} [cm^{-1}] = 3058, 2866, 2787, 1958, 1649, 1562, 1434(s), 1389(m), 1347, 1302(m), 1234, 1193, 1147, 1062, 1042, 996, 886, 790(m), 738, 725, 681, 567, 523. Anal. calcd. for $C_{22}H_{18}Cl_4IrN_3O$: C, 39.18; H, 2.69; N, 6.23. Found: C, 39.29; H, 2.97; N, 6.10.

Synthesis of [Ir(Cl$_4$N$_3$)N$_3$] (4-Cl). A solution of 237 mg (351 µmol) of complex [Ir(Cl$_4$N$_3$)OMe] (**3**) in 7 ml of THF and a solution of 85 µl (82 mg, 710 µmol) trimethylsilylazide in 2 ml of THF were cooled separately in scintillation vials to –35 °C. The cold azide solution was then added dropwise to the cold, stirred solution of complex **3**. The resulting reaction solution was stored at –35 °C for 2.5 h. The solvent was then removed in vacuum and the remaining volatiles were co-evaporated with 5 ml of pentane. After drying the solid in vacuum for 4 h, the green product was obtained in 91% yield (220 mg, 321 µmol). Because of the thermal instability of **4-Cl**, elemental analysis was not attempted. ^{1}H NMR (400 MHz, THF-d_8): δ = 8.74 (t, 1H, ^3J = 7.9 Hz, $C_{py}\boldsymbol{H}(4)$); 8.37 (d, 2H, ^3J = 7.9 Hz, $C_{py}\boldsymbol{H}(3,5)$); 7.53 (d, 4H, ^3J = 8.2 Hz, $C_{arom}\boldsymbol{H}(3,5)$); 7.26 (t, 2H, ^3J = 8.1 Hz, $C_{arom}\boldsymbol{H}(4)$); 0.69 (s, 6H, NC-C$\boldsymbol{H}_3$) ppm. ^{13}C{1H} NMR (100 MHz, THF-d_8): δ = 173.9 ($\boldsymbol{C}$=N); 162.8 ($\boldsymbol{C}_{py}(2,6)$); 151.1 ($\boldsymbol{C}_{arom}(1)$); 129.8 ($\boldsymbol{C}_{arom}(2,6)$); 129.6 ($\boldsymbol{C}_{arom}(3,5)$); 129.0 ($\boldsymbol{C}_{arom}(4)$); 125.3 ($\boldsymbol{C}_{py}(3,5)$); 122.5 ($\boldsymbol{C}_{py}(4)$); 20.5 (NC-$\boldsymbol{C}H_3$) ppm. IR (KBr): ν_{max} [cm^{-1}] = 3067(w), 2920(w), 2872, 2034(vs) ($\nu_{asym}(N_3)$), 1638, 1562, 1476, 1436(m), 1408, 1379, 1349,

1317, 1295, 1272, 1234, 1143, 1044, 790, 773, 728, 680. UV/vis (KBr): λ_{max} [nm] = 435, 492, 523, 820, 981.

Synthesis of [Ir(Cl$_4$N$_3$)^{15}N═N$_3$/N$_2$═^{15}N] (4-Cl-^{15}N). The synthesis of the ^{15}N labeled azido isotopologue (**4-Cl-^{15}N**) was performed analogous to the unlabeled complex (**4-Cl**) with in situ prepared (CH$_3$)$_3$Si^{15}N═N$_2$/N$_2$═^{15}N (50/50) as previously described.[4] IR (KBr): ν_{max} [cm^{-1}] = 3067(w), 2920(w), 2027(vs) (ν_{asym}(^{14}N$_2$^{15}N)), 2017(vs) (ν_{asym}(^{15}N^{14}N$_2$)), 1562, 1477, 1435(m), 1407, 1381, 1350, 1333, 1296, 1251, 1234, 1143, 1070, 1044, 995, 790, 774, 727, 680.

Synthesis of [Ir(Me$_4$N$_3$)N$_3$] (4-Me). A solution of 221 mg (373 µmol) of the complex [Ir(Me$_4$N$_3$)OMe] in 8 ml of THF and a solution of 99 µl (86 mg, 0.75 mmol) trimethylsilylazide in 3 ml of THF were cooled separately in scintillation vials to −35 °C. The cold azide solution was then added dropwise to the cold, stirred solution of the iridium methoxido complex. The resulting reaction solution was stored at −35 °C for 3 h. The solvent was then removed in vacuum and the remaining volatiles were co-evaporated 3 times with 3 ml of pentane. After drying the solid in vacuum for several hours, the brown/green product was obtained in 90% yield (203 mg, 336 µmol). Because of the thermal instability of **4-Me**, elemental analysis was not attempted. ^{1}H NMR (200 MHz, THF-d_8): δ = 8.61 (t, 1H, ^3J = 7.9 Hz, C$_{py}$***H***(4)); 8.08 (d, 2H, ^3J = 7.9 Hz, C$_{py}$***H***(3,5)); 7.17–7.01 (m, 6H, C$_{arom}$***H***(3,4,5)); 2.04 (s, 12H, C***H***$_3$); 0.97 (s, 6H, NC-C***H***$_3$) ppm. ^{13}C{1H} NMR (100 MHz, THF-d_8): δ = 171.7 (***C***═N); 162.7 (***C***$_{py}$(2,6)); 153.6 (***C***$_{arom}$(1)); 131.0 (***C***$_{arom}$(2,6)); 129.1 (***C***$_{arom}$(3,5)); 127.1 (***C***$_{arom}$(4)); 123.8 (***C***$_{py}$(3,5)); 121.9 (***C***$_{py}$(4)); 18.9 (***C***H$_3$); 18.6 (NC-***C***H$_3$) ppm. IR (KBr): ν_{max} [cm^{-1}] = 3064, 3025, 2954w, 2918w, 2038vs (ν_{as}(N$_3$)), 1591, 1469 m, 1443w, 1380 m, 1352, 1314 m, 1294, 1218, 1174, 1165, 1165, 1092, 1047, 991, 841w, 776m. UV/vis (THF): λ_{max} [nm] = 334, 430, 493, 589, 650, 800.

DSC assisted synthesis of [Ir(Cl$_4$N$_3$)N] (6-Cl). Between 4 and 9 mg (6–13 µmol) of the complex [Ir(Cl$_4$N$_3$)N$_3$] (**4-Cl**) were placed in aluminum pans for DSC measurements and the pans were sealed under a nitrogen atmosphere. The pans were opened with a needle and the samples were then directly measured with a Netzsch DSC 204 F1 instrument in cycles between 50 and 90 °C. The measurement was stopped when no additional reaction enthalpy could be detected. IR (KBr): ν_{max} [cm^{-1}] = 3070, 2975, 2870, 2036, 1951, 1636, 1561, 1434(m), 1366, 1345, 1286(s), 1243, 1135, 1094, 1046, 993, 955 (IrN), 891, 788, 737, 685, 552. UV/vis (KBr): λ_{max} [nm] = 466, 593, 770, 836. Anal. calcd. for C$_{21}$H$_{15}$Cl$_4$IrN: C, 38.37; H, 2.30; N, 8.52. Found: C, 38.94; H, 2.38; N, 8.30.

Synthesis of [Ir(Cl$_4$N$_3$)N] (6-Cl), batch. In a Schlenk tube, fitted with a J. Young teflon valve, 85 mg (126 µmol) **4-Cl** were placed under vacuum. The Schlenk tube was sealed and heated up to 90 °C for one hour.

Synthesis of [Ir(Cl$_4$N$_3$)^{14}N/^{15}N] (6-Cl-^{15}N). The synthesis of the ^{15}N labeled nitrido complex (**6-Cl-^{15}N**) was performed analogous to the unlabeled complex **6-Cl** with a Netzsch DSC 204 F1 instrument in cycles between 50 and 90 °C. IR (KBr): ν_{max} [cm^{-1}] = 3070, 2914, 2026, 1951, 1636, 1561, 1435(m), 1345, 1285(m), 1242, 1135, 1094, 1070, 1022, 992, 955 (Ir^{14}N), 925 (Ir^{15}N), 891, 788, 738, 685, 552.

Thermolysis of [Ir(Cl$_4$N$_3$)N] (6-Cl). A solid sample of 30 mg (46 µmol) of complex [Ir(Cl$_4$N$_3$)N] (**6-Cl**) was placed in a Schlenk tube equipped with a J. Young Teflon valve. The sample was then placed under vacuum, the Schlenk tube was closed and heated to 150 °C for 19 h. Anal. calcd. for C$_{21}$H$_{15}$Cl$_4$IrN: C, 38.37; H, 2.30; N, 8.52. Found: C, 38.72; H, 2.44; N, 8.43.

NMR scale reaction of [Ir(Cl$_4$N$_3$)N] (6-Cl) with Ph$_3$SiH or Et$_3$SiH. A solution of either Ph$_3$SiH or Et$_3$SiH (*ca.* 0.23 mmol) in 0.5 ml of THF-d_8 was added to a solid sample of the complex [Ir(Cl$_4$N$_3$)N] (*ca.* 15 mg, 0.023 mmol) containing *ca.* 5 mg (0.027 mmol) of ferrocene as an internal standard. The resulting suspension was stirred for 2–3 min and then filtered. The residue was extracted with 0.2 ml of THF-d_8, the combined THF-d_8 solutions were placed in a NMR tube and a ^{1}H NMR spectrum was recorded. From integration of the ^{1}H NMR product signals against the resonance of ferrocene, yields of 40–90% and 30–50% for Ph$_3$SiH and Et$_3$SiH were estimated.

Reaction of [Ir(Cl$_4$N$_3$)N] (6-Cl) with Et$_3$SiH. A solution of 95 µl (69 mg, 0.59 mmol) of Et$_3$SiH in 10 ml of THF was added to 41 mg (61 µmol) of the solid complex [Ir(Cl$_4$N$_3$)N] (**6-Cl**). This resulted in a brown solution, which was stirred for 10 min. The solvent was removed in vacuum and the residue was extracted into Et$_2$O. The Et$_2$O phase was removed in vacuum, the remaining volatiles were co-evaporated with 1 ml of pentane and the solid was dried for *ca.* 5 h in vacuum. 29 mg of a brown solid were obtained, which according to ^{1}H NMR analysis were mainly consistent of complex **9**. All attempts to re-crystallize the complex were so far unsuccessful or resulted in decomposition of the complex. ^{1}H NMR (400 MHz, C$_6$D$_6$): δ = 8.20 (d, 2H, ^3J = 7.9 Hz, C$_{py}$***H***(3,5)); 8.06 (s, 1H, N***H***); 7.64 (t, 1H, ^3J = 7.0 Hz, C$_{py}$***H***(4)); 7.11 (d, 4H, ^3J = 8.1 Hz, C$_{arom}$***H***(3,5)); 6.63 (t, 2H, ^3J = 8.1 Hz, C$_{arom}$***H***(4)); 1.03 (t, 9H, ^3J = 7.9 Hz, Si(CH$_2$C***H***$_3$)$_3$); 0.41 (q, 6H, ^3J = 7.9 Hz, Si(C***H***$_2$CH$_3$)$_3$); 0.19 (s, 6H, NC-C***H***$_3$) ppm. ^{1}H-^{15}N HSQC (400 MHz/41 MHz, C$_6$D$_6$): δ = 127 (***N***H) ppm.

Synthesis of [Ir(Cl$_4$N$_3$)N(H)SiPh$_3$] (10). A solution of 34 mg (131 µmol) of triphenylsilane in 6 ml of toluene was added to a solid sample of 77 mg (117 µmol) of the complex [Ir(Cl$_4$N$_3$)N] (**6-Cl**). The resulting suspension was stirred for 25 min, upon which most of the solid material dissolved, leading to a brown–green colour of the supernatant. The suspension was filtered and the residue was extracted with 1.5 ml of toluene. The solvent was removed in vacuum and the resulting solid was co-evaporated three times with 1.5 ml of pentane. The raw product was then washed in 1.5 ml portions with a total of 20 ml of pentane. The residue was then extracted into Et$_2$O and filtered. The Et$_2$O was removed in vacuum and the washing/extracting procedure was repeated. The product was recrystallized twice from an Et$_2$O solution layered with pentane at −35 °C, yielding 8 mg (9 µmol; 8%) of the green complex **10**. Single crystals suitable for X-ray diffraction analysis were obtained from an Et$_2$O solution at −35 °C after several month. ^{1}H NMR (400 MHz, THF-d_8): δ = 8.68 (d, 2H, ^3J = 7.9 Hz, C$_{py}$***H***(3,5)); 8.25 (t, 1H, ^3J = 7.9 Hz, C$_{py}$***H***(4)); 7.22 (s(br), 1H, N***H***); 7.33–7.29 (m, 6H, C$_{phenyl}$***H***(2,6)); 7.18–713 (m, 3H, C$_{phenyl}$***H***(4)); 7.11–7.06 (m, 6H, C$_{phenyl}$***H***(3,5)); 6.89 (m, 4H, C$_{arom}$***H***(3,5)); 6.74 (m, 4H, C$_{arom}$***H***(4)); 0.47 (s, 6H, NC-C***H***$_3$) ppm. ^{13}C{^{1}H} NMR (100 MHz, THF-d_8): δ = 167.2 (***C***═N); 159.3 (***C***$_{py}$(2,6)); 150.8 (***C***$_{arom}$(1)); 142.7 (***C***$_{phenyl}$(1)); 136.9 (***C***$_{phenyl}$(2,6));

130.1 (C_{arom}(2,6)); 129.1, 128.9, 128.4, 127.7 (C_{arom}(3,5), C_{arom}(4), C_{phenyl}(3,5), C_{phenyl}(4)); 124.0 (C_{py}(3,5)); 118.2 (C_{py}(4)); 20.8 (NC-CH_3) ppm. ^{1}H-^{15}N HSQC (400 MHz/41 MHz, THF-d_8) δ [ppm]: 104 (Ir*N*H-SiPh$_3$). ^{1}H-^{29}Si HMBC (400/79 MHz, THF-d_8) δ [ppm]: −16 (IrNH-*Si*Ph$_3$). Anal. calcd. for $C_{39}H_{31}Cl_4IrN_4Si$: C, 51.04; H, 3.40; N, 6.10. Found: C, 50.31; H, 3.42; N, 5.98.

VT NMR measurement of [Ir(Cl$_4$N$_3$)N(H)SiPh$_3$] (10). 3 mg (3 μmol) of complex **10** were dissolved in 0.7 ml of THF-d_8. The solution was transferred to a NMR tube fitted to a Cajoin ultravacuum adapter attached to a J. Young high vacuum tap. The NMR tube was then transferred to a high vacuum manifold, the solution was frozen in liquid nitrogen and the NMR tube was flame sealed under vacuum. The solution was thawed by shaking the NMR tube at −100 °C in an EtOH/N_2 coldbath. The NMR tube was then transferred to the pretempered NMR probe. ^{1}H NMR spectra were recorded from −100 °C to −50 °C in 10 °C steps.

Computational Studies

The DFT calculations were carried out with the parallelized versions 6.2 of Turbomole[22] on our 192 and 80 core Intel Harpertown and Nehalem clusters. The geometries of the ground and transition states were optimized without symmetry restrictions (C_1-symmetry). The complexes described herein were probed for singlet and triplet states S = 0 and 1 using unrestricted calculations. They were characterized as stationary points by the calculation of analytical second derivatives through the absence (ground states) or presence of one imaginary frequency (transition states). The transition states were further analyzed by IRC calculations, which assured the correctness of the reaction paths. For the latter, the Gaussian 03 geometry optimizer[23] was used in combination with a perl script (Gau_external written by Karin Wichmann) interfacing to Turbomole. Additionally a perl script graciously provided by Dr Armin Hellweg from COSMOlogic GmbH & Co. KG was utilized for the calculation of IRC paths.

The Becke-Perdew (BP-86) functional[24] was used for the geometry optimizations employing the resolution of identity (RI) methodology[25] available in Turbomole (ridft, rdgrad). The modified grids, m3 and m4, available in Turbomole were employed for the DFT calculations.

The dependence of the energetics (thermodynamics and barriers) on the DFT functionals and the basis set dependence was previously probed for related systems[4,11] and evidenced only negligible deviations. We therefore refrained from the assessment of the performance of the DFT functionals and basis sets for the systems described herein. For the iridium center a Stuttgart-Dresden pseudopotential (ECP-28-MWB- and ECP-60-MWB) was used throughout.[26] The employed DFT functional and basis sets are provided along with the optimized geometries in the ESI†.

Conclusions

The chloride protection of potential ligand sites amenable to C–H activation allowed us isolate a terminal nitrido complex **6-Cl** with sterically less demanding groups. The low solubility in organic solvents thwarted the full characterization of the nitrido compound. Its reaction with silanes to give the corresponding silyl amido complexes provided however good evidence for the assigned structure with a terminal nitrido unit. Currently, we are in the process to synthesize related complexes with chloro protected ligands of higher solubility and will report their chemistry in due course. Mechanistic aspects of silane addition to iridium nitrido units to produce amido complexes will be discussed in detail in a separate forthcoming publication.

Acknowledgements

Funding by Deutsche Forschungsgemeinschaft is gratefully acknowledged. The authors are indebted to Prof. Ulrich Behrens for assistance at the final stage of the crystal structure analysis and Dr Thomas Hackl for helpful discussions concerning lineshape analysis. The authors would like to thank Uta Sazama and Sandra Maracke for DSC and DTG/MS measurements and Eike Anheier, Jan-Moritz Adam and Matthias Schreyer for assistance with the syntheses.

Notes and references

1 J. F. Berry, *Comments Inorg. Chem.*, 2009, **30**, 28–66.
2 A. Walstrom, M. Pink, X. Yang, J. Tomaszewski, M.-H. Baik and K. G. Caulton, *J. Am. Chem. Soc.*, 2005, **127**, 5330–5331.
3 (*a*) C. Vogel, F. Heinemann, J. Sutter, C. Anthon and K. Meyer, *Angew. Chem., Int. Ed.*, 2008, **47**, 2681–2684; (*b*) J. J. Scepaniak, M. D. Fulton, R. P. Bontchev, E. N. Duesler, M. L. Kirk and J. M. Smith, *J. Am. Chem. Soc.*, 2008, **130**, 10515–10517.
4 J. Schöffel, A. Yu Rogachev, S. DeBeer George and P. Burger, *Angew. Chem., Int. Ed.*, 2009, **48**, 4734–4738.
5 T. A. Betley and J. C. Peters, *J. Am. Chem. Soc.*, 2004, **126**, 6252–6254.
6 J.-U. Rohde, T. A. Betley, T. A. Jackson, C. T. Saouma, J. C. Peters and L. Que, *Inorg. Chem.*, 2007, **46**, 5720–5726.
7 J. Scepaniak, J. Young, R. Bontchev and J. Smith, *Angew. Chem., Int. Ed.*, 2009, **48**, 3158–3160.
8 (*a*) W.-L. Man, W. W. Y. Lam, H.-K. Kwong, S.-M. Peng, W.-T. Wong and T.-C. Lau, *Inorg. Chem.*, 2010, **49**, 73–81; (*b*) X.-Y. Yi, H.-Y. Ng, I. D. Williams and W.-H. Leung, *Inorg. Chem.*, 2011, **50**, 1161–1163.
9 Y. Badiei, A. Dinescu, X. Dai, R. Palomino, F. Heinemann, T. Cundari and T. Warren, *Angew. Chem., Int. Ed.*, 2008, **47**, 9961–9964.
10 (*a*) C. Ni, J. C. Fettinger and P. P. Power, *Organometallics*, 2010, **29**, 269–272; (*b*) A. K. Musch Long, R. P. Yu, G. H. Timmer and J. F. Berry, *J. Am. Chem. Soc.*, 2010, **132**, 12228–12230; (*c*) C. C. H. Atienza, A. C. Bowman, E. Lobkovsky and P. J. Chirik, *J. Am. Chem. Soc.*, 2010, **132**, 16343–16345.
11 J. Schöffel, N. Šušnjar, S. Nückel, D. Sieh and P. Burger, *Eur. J. Inorg. Chem.*, 2010, 4911–4915.
12 Y. Chen, R. Chen, C. Qian, X. Dong and J. Sun, *Organometallics*, 2003, **22**, 4312–4321.
13 (*a*) A. Mentes, J. Fawcett and R. D. W. Kemmitt, *Acta Crystallogr., Sect. E: Struct. Rep. Online*, 2001, **57**, o424–o425; (*b*) Y.-B. Huang, X.-L. Ma, S.-N. Zheng, J.-X. Chen and C.-X. Wei, *Acta Crystallogr., Sect. E: Struct. Rep. Online*, 2006, **62**, o3044–o3045.
14 H. F. Haarman, J. M. Ernsting, M. Kranenburg, H. Kooijman, N. Veldman, A. L. Spek, P. W. N. M. van Leeuwen and K. Vrieze, *Organometallics*, 1997, **16**, 887–900.
15 E. L. Dias, M. Brookhart and P. S. White, *Organometallics*, 2000, **19**, 4995–5004.
16 S. Nückel and P. Burger, *Organometallics*, 2001, **20**, 4345–4359.
17 The residues of some of the batch reactions dissolved partially in THF. However, the UV/vis and IR spectra of the THF extracted material are different to the spectra of the solid samples from which they have been obtained (*cf.* ESI†). This suggests that the extracted compounds are minor impurities or decomposition products.
18 M. A. Arthurs, J. Bickerton, S. R. Stobart and J. Wang, *Organometallics*, 1998, **17**, 2743–2750.
19 R. R. Cramer, J. A. McCleverty and J. Bray, *Inorg. Synth.*, 1990, **28**, 86–88.
20 G. M. Sheldrick, *Acta Crystallogr., Sect. A: Found. Crystallogr.*, 2007, **64**, 112.
21 L. J. Farrugia, *J. Appl. Crystallogr.*, 1997, **30**, 568.

22 TURBOMOLE V6.2 2010, a development of University of Karlsruhe and TURBOMOLE GmbH since 2007, available from http://www.turbomole.com.
23 *Gaussian 03*, Revision C.02, M. J. Frisch, G. W. Trucks, H. B. Schlegel, G. E. Scuseria, M. A. Robb, J. R. Cheeseman, J. A. Montgomery, Jr., T. Vreven, K. N. Kudin, J. C. Burant, J. M. Millam, S. S. Iyengar, J. Tomasi, V. Barone, B. Mennucci, M. Cossi, G. Scalmani, N. Rega, G. A. Petersson, H. Nakatsuji, M. Hada, M. Ehara, K. Toyota, R. Fukuda, J. Hasegawa, M. Ishida, T. Nakajima, Y. Honda, O. Kitao, H. Nakai, M. Klene, X. Li, J. E. Knox, H. P. Hratchian, J. B. Cross, V. Bakken, C. Adamo, J. Jaramillo, R. Gomperts, R. E. Stratmann, O. Yazyev, A. J. Austin, R. Cammi, C. Pomelli, J. W. Ochterski, P. Y. Ayala, K. Morokuma, G. A. Voth, P. Salvador, J. J. Dannenberg, V. G. Zakrzewski, S. Dapprich, A. D. Daniels, M. C. Strain, O. Farkas, D. K. Malick, A. D. Rabuck, K. Raghavachari, J. B. Foresman, J. V. Ortiz, Q. Cui, A. G. Baboul, S. Clifford, J. Cioslowski, B. B. Stefanov, G. Liu, A. Liashenko, P. Piskorz, I. Komaromi, R. L. Martin, D. J. Fox, T. Keith, M. A. Al-Laham, C. Y. Peng, A. Nanayakkara, M. Challacombe, P. M. W. Gill, B. Johnson, W. Chen, M. W. Wong, C. Gonzalez and J. A. Pople, Gaussian, Inc., Wallingford CT, 2004.
24 (*a*) A. D. Becke, *Phys. Rev. A: At., Mol., Opt. Phys.*, 1988, **38**, 3098; (*b*) J. P. Perdew, *Phys. Rev. B*, 1986, **33**, 8822.
25 O. Treutler and R. Ahlrichs, *J. Chem. Phys.*, 1995, **102**, 346.
26 D. Andrae, U. Haeussermann, M. Dolg, H. Stoll and H. Preuss, *Theor. Chim. Acta*, 1990, **77**, 1431.

